Pharm Res (2012) 29:722–738
DOI 10.1007/s11095-011-0597-0

RESEARCH PAPER

# Characterization of Recombinant Human IL-15 Deamidation and Its Practical Elimination through Substitution of Asparagine 77

David F. Nellis • Dennis F. Michiel • Man-Shiow Jiang • Dominic Esposito • Richard Davis • Hengguang Jiang • Angela Korrell • George C. Knapp IV • Lauren E. Lucernoni • Roy E. Nelson • Emily M. Pritt • Lauren V. Procter • Mark Rogers • Terry L. Sumpter • Vinay V. Vyas • Timothy J. Waybright • Xiaoyi Yang • Amy M. Zheng • Jason L. Yovandich • John A. Gilly • George Mitra • Jianwei Zhu

Received: 28 July 2011 / Accepted: 14 September 2011 / Published online: 19 October 2011


## ABSTRACT

***Purpose*** The use of recombinant human interleukin (rhIL)-15 as a potential therapeutic immune modulator and anticancer agent requires pure, stable preparations. However, purified rhIL-15 preparations readily accumulated heterogeneities. We sought to improve rhIL-15 stability through process, formulation, and targeted amino acid changes.

***Methods*** The solution state of rhIL-15 *versus* buffer composition and temperature was studied using SEC and IEX methods. rhIL-15 deamidation was confirmed using RP-HPLC/ESI-MS, enzymatic labeling, and peptide mapping. Deamidation kinetics were measured *versus* buffer composition and pH using RP-HPLC. Deamidation-resistant rhIL-15 variants (N77A, N77S, N77Q, G78A, and [N71S/N72A/N77A]) were produced in *E. coli*, then assayed for T-cell culture expansion potency and deamidation resistance.

***Results*** Adding 20% ethanol to buffers or heating at ≥32°C dispersed rhIL-15 transient pairs, improving purification efficiencies. Asparagine 77 deamidated rapidly at pH 7.4 with activation energy of 22.9 kcal per mol. Deamidation in citrate buffer was 17-fold slower at pH 5.9 than at pH 7.4. Amino acid substitutions at N77 or G78 slowed deamidation ≥23-fold. rhIL-15 variants N77A and (N71S/N72A/N77A) were active in a CTLL-2 proliferation assay equivalent to unsubstituted rhIL-15.

***Conclusions*** The N77A and (N71S/N72A/N77A) rhIL-15 variants are resistant to deamidation and remain potent, thus providing enhanced drug substances for clinical evaluation.

**KEY WORDS** competing equilibria · deamidation · interleukin-15 · kinetics · protein engineering

## ABBREVIATIONS

| | |
|---|---|
| ATCC | American Type Culture Collection |
| BTP | 1,3-Bis[tris(hydroxymethyl)methylamino]propane |
| C/N | catalog number |
| d | days |
| DNS | data not shown |
| DTT | dithiothreitol |

D. F. Nellis • D. F. Michiel • M.-S. Jiang • H. Jiang • A. Korrell • G. C. Knapp IV • L. E. Lucernoni • R. E. Nelson • E. M. Pritt • T. L. Sumpter • V. V. Vyas • X. Yang • A. M. Zheng • J. A. Gilly • G. Mitra • J. Zhu (✉)
Biopharmaceutical Development Program, SAIC-Frederick, Inc.
National Cancer Institute at Frederick
Frederick, Maryland 21702, USA
e-mail: zhujianwei@mail.nih.gov

D. Esposito • L. V. Procter
Protein Expression Laboratory, Advanced Technology Program
National Cancer Institute at Frederick
Frederick, Maryland 21702, USA

R. Davis • M. Rogers
M-Scan, Inc., 606 Brandywine Parkway
West Chester, Pennsylvania 19380, USA

T. J. Waybright
Laboratory of Proteomics and Analytical Technologies
Advanced Technology Program
National Cancer Institute at Frederick
Frederick, Maryland 21702, USA

J. L. Yovandich
Biological Resources Branch
National Cancer Institute at Frederick
Frederick, Maryland 21702, USA

| | |
|---|---|
| EDTA | ethylenediaminetetraacetic acid |
| ESI-MS | electrospray ionization mass spectrometry |
| FBS | fetal bovine serum |
| F- | formulation |
| HPLC | high-performance liquid chromatography |
| HEPA | high-efficiency particulate air filter |
| HIC | hydrophobic interaction chromatography |
| i.d. | inner diameter |
| IB | inclusion bodies |
| IEX | ion-exchange chromatography |
| IPTG | isopropyl β-D-1-thiogalactopyranoside |
| MS/MS | collision fragmentation mass spectrometry |
| QToF | quadrupole time-of-flight mass spectrometry |
| PIMT | protein isoaspartate methyltransferase |
| rhIL-15 | recombinant human interleukin-15 |
| RP | reverse phase |
| rpm | rotations per minute |
| SDS-PAGE | sodium dodecyl sulfate-polyacrylamide gel electrophoresis |
| SEC | size exclusion chromatography |
| TFA | trifluoroacetic acid |
| UPLC | ultra-high performance liquid chromatography |

## INTRODUCTION

IL-15 is a naturally occurring cytokine that influences cellular immune responses and contributes to the proper functioning of the mammalian immune system (1). For instance, IL-15 slows viral replication by stimulating macrophage release of nitric oxide and regulates contraction-phase dynamics to increase the number of $CD8^+$ T cells converted into memory cells (2). Participants at a July 2007 National Cancer Institute's Immunotherapy Agent Workshop ranked IL-15 as first among 20 immune modulators having the potential utility to treat cancer (3). While IL-15 has been difficult to produce in larger quantities using mammalian cell expression systems, the substantial interest in IL-15 has motivated the $(his)_6$-tagged / enterokinase-cleaved recovery of refolded rhIL-15 from *E. coli* inclusion bodies (4) as well as the non-tagged production of GMP-compliant clinical supplies of rhIL-15 (5,6). Recent review articles demonstrate that interest in developing the therapeutic potential of IL-15 remains vigorous (7,8). Supplies of stable, high-purity recombinant human IL-15 (rhIL-15) are necessary for human clinical trials. In this context, continued improvement of methods for rhIL-15 production is of current interest.

Peptides and proteins can rapidly degrade in a sequence-dependent manner through deamidation, a chemical reaction that exchanges amide nitrogen groups with oxygen (9–13). Deamidation introduces heterogeneity into a protein by changing asparagine or glutamine side chains from uncharged, polar amides into negatively charged carboxylic acids. This change impacts protein surface hydrophobicity and surface-charge density. rhIL-2, another cytokine sharing some properties with rhIL-15, was reported to maintain its activity after deamidation (14); however, deamidation in therapeutic human hormone preparations of oxytocin and insulin changed the biological potency of the formulated drugs (15,16). The potential for a range of spontaneous post-translational modifications to elicit autoantigenicity has been recently reviewed (17). For instance, cytochrome c peptide fragments with either aspartic or an isoaspartic acid residue showed differential immunogenicity (18). For rhIL-15, it is theoretically possible that immune responses against deamidated rhIL-15 forms could provoke cross-reactive responses against endogenous rhIL-15, potentially impacting immune system function. Because a non-deamidated protein is chromatographically similar to its deamidated forms, stringent demands are placed on manufacturing processes used to isolate the non-deamidated therapeutic protein. Therefore, by minimizing rhIL-15 deamidation, in addition to elimination of a potential autoantigenicity mode, improvements in processing efficiency, drug quality, and product stability would be realized.

We report structural improvements to rhIL-15 that provide resistance to deamidation while maintaining its *in vitro* potency. These improvements were designed after characterizing rhIL-15 deamidation kinetics. Suppression of transient rhIL-15 pairing improved chromatographic separations, showed that rhIL-15 dimer formation was not a major contributor to preparation heterogeneity, and facilitated efficient rhIL-15 production. The extent of rhIL-15 degradation instability *versus* temperature was quantified by calculating the rhIL-15 deamidation reaction's Arrhenius activation energy. rhIL-15 deamidation kinetics were measured under a range of buffer and pH conditions. This information enabled rhIL-15 to be partially stabilized through handling and formulation. However, for therapeutic use it is highly desirable to create improved forms of rhIL-15 to minimize deamidation. A single amino acid, asparagine-77, was analytically identified as the primary site of observed rhIL-15 deamidation. Through construction of genetic variants, rhIL-15 was fortified against deamidation by substitution at asparagine-77 or glycine-78. Marginal additional stability was conferred by substitution at asparagines 71 and 72. Two rhIL-15 variants, rhIL-15 N77A and rhIL-15-(N71S/N72A/N77A), were compared with unsubstituted rhIL-15 and shown to have equivalent CTLL-2 cell proliferation potencies. Thus, transient pair suppression combined with N77x rhIL-15 variants provided an enhanced approach to manufacturing rhIL-15 preparations for clinical study.

## MATERIALS AND METHODS

### SDS-PAGE

Guanidine-containing samples were prepared by cold ethanol precipitation (19). Then, samples in reducing SDS-NuPAGE sample buffer (5% 2-mercaptoethanol) were heated to 95°C for 10 min, loaded onto 4–12% Bis-Tris NuPAGE gels (Invitrogen, CA), developed for 45 min at 200 V, stained with SyproRuby (Invitrogen), fluorescence-scanned (Molecular Dynamics, Model 595 GE Healthcare), and processed with ImageMaster 1D Elite software, version 4.1 (GE Healthcare).

### PIMT Assay

Protein isoaspartate methyltransferase specifically methylates isoaspartic acid residues. Reactions were performed as per the kit manufacturer's instructions (ISOQUANT Isoaspartate Detection Kit, MA1010, Promega, Madison, WI), except for use of 500 mM sodium phosphate reaction buffer, pH 6.8, to minimize X-114 detergent peaks in ExRP-HPLC profiles.

### RP-HPLC

Deamidation was initially characterized using an expanded resolution reverse phase HPLC method (ExRP-HPLC). An Agilent HPLC system (Agilent, Santa Clara, CA) with temperature-controlled injector and column compartments, held at either 10°C or 20°C, was fitted with two tandem-plumbed C18-columns (X-Bridge BEH300, C18, 3.5 μm, 250 mm, Waters, Milford, MA). Mobile phases were 0.08% TFA and 0.02% formic acid in HPLC-grade water or acetonitrile. Elution was performed at 0.5 ml/min with 4.6-mm columns or at 0.14 ml/min with 2.1-mm columns and monitored at 210 nm (min-%B: 0–0; 12–0; 16–47; 116–53; 126–100; 128–100; 130–0; 142–0). Variant impurity profiles and deamidation kinetics were measured using a faster RP-HPLC method. Tandem columns (Poroshell 300SB-C8, 5 μm, 2.1×75 mm, Agilent, 15°C) were eluted (0.08% TFA, 0.02% formic acid, in either HPLC-grade water or 4:1 acetonitrile:isopropanol) at 0.5 ml/min (min-%B: 0–0; 4.5–50; 64–65; 65–100; 67–0; 68–0), and monitored at 210 nm. For both columns/methods, early peak edges and peak maxima shifted to earlier elution times with increased peak mass loading. However, the retention times of the later-eluting peak tail inflection times were independent of peak loading and thus characteristic of each analyte. Peak areas were integrated using Agilent ChemStation Software.

### SEC-HPLC

Mobile phase buffers were prepared in either water or 30% ethanol, starting from 10× PBS (0.17M $KH_2PO_4$, 0.5M $Na_2HPO_4$, 1.5M NaCl, pH 7.4). Samples were chilled prior to injection (25 μl) onto the column (G2000SW, 5 μm, 0.78×30 cm, Tosoh Biosciences, King of Prussia, PA), and elution was monitored at 280 nm. Gel filtration standards (BioRad Laboratories, Hercules, CA) were run as controls. Temperature scouting was run at 0.75 ml/min with an aqueous mobile phase, while solvent scouting was run at 0.375 ml/min and 22°C with various ethanol percentages. rhIL-15 variant monomer percentages were assayed at 0.375 ml/min with 1× PBS in 20% ethanol at 22°C; or with 1× PBS in water at 37°C.

### IEX-HPLC

Using Source 15Q resin (15 μm, GE Healthcare, Piscataway, NJ) in an analytical column (Tricorn 5/250, 5×200 mm, GE Healthcare), IEX-HPLC profile variations with temperature changes were studied. Buffers were prepared in water (A: 7 mM BTP, 7 mM NaCl, pH 6.8; B: 14 mM BTP, 700 mM NaCl, pH 6.8) and the column was developed with a linear salt gradient over 78 min. For study of ethanol impacts on IEX-HPLC profiles, a polymeric column (Pro-Pak SAX-10, 10 μm, 4×250 mm, Dionex, Sunnyvale, CA) was run at 1 ml/min and 25°C. For solvent addition scouting, buffers were prepared in either water or 30% ethanol (A: 7 mM BTP, 7 mM NaCl, pH 6.8; B: 14 mM BTP, 700 mM NaCl, pH 6.8). Salt gradients having fixed ethanol percentages were produced using four-inlet mixing. The column was developed with a linear salt gradient from 7 to 700 mM NaCl over 39 min and monitored at 280 nm.

### Peptide Mapping

Samples with approximately 65% deamidation, as determined by ExRP-HPLC, were digested in 25 mM sodium phosphate, 500 mM NaCl, pH 7.4, with sequencing-grade chymotrypsin at a protein/enzyme ratio of 1:20 for 4 h at 37°C. The digested samples were reduced with DTT for 1 h at 37°C. The digest (100 μl) was resolved using an Agilent 1100 Binary HPLC fitted with a TSKgel Super-ODS column (G0020-95F, 35°C, 2 μm, 2.0×50 mm, Tosoh Bioscience) and buffers with 0.1% TFA in HPLC water or acetonitrile (buffer B). The column was developed at 0.4 ml/min (min-%B: 0–2; 2–2; 30–60; 40–100; 45–100) and the eluted peptides were monitored at 214 nm, followed by ESI-MS, using a MicroMass Q-ToF API US quadrupole time-of-flight mass spectrometer (Waters) operating in positive ion mode. Selected peptides were analyzed by on-line MS/MS with nitrogen as the collision gas and the collision energy varied to produce the daughter ion spectrum.

## Deamidation Kinetics

rhIL-15 reference standard was formulated in 25 mM sodium phosphate, 500 mM NaCl, pH 7.4, and incubated at temperatures between 6 and 40°C, in 5°C increments, and analyzed at intervals using ExRP-HPLC. Individual deamidation ratio measurements were plotted *versus* injection time and fit to single-component exponential decay curves of the formula $Y_t = Y_O \bullet e^{-At}$, where "t" is the incubation time in days and "A" is the first-order degradation constant, using a weighted least squares method (Trendline function, Microsoft Excel 2000). In accordance with the classical Arrhenius equation, $\ln(k_T) = \ln(A) - -(E_a/R) \times (1/T)$, where "$k_T$" is the deamidation rate, "A" is the pre-exponential factor, "$E_a$" is Arrhenius activation energy [cal $mol^{-1}$], "R" is molar gas constant (1.985 [cal $K^{-1}$ $mol^{-1}$]), and "T" is the thermodynamic temperature (K), as described in greater detail by Hawe and co-workers (15). The natural logarithm of each deamidation rate constant was plotted *versus* the reciprocal thermodynamic temperature. The linear regression slope was used to calculate the Arrhenius activation energy.

## rhIL-15 Formulation Survey

The rhIL-15 reference standard was buffer-exchanged into water (PD-10 column, GE Healthcare), 0.2-μm filtered, and distributed (50-μl aliquots) into autoclaved, polypropylene injection vials. The pH values of 10-fold buffer/salt formulation stocks were adjusted to obtain the target pH values upon dilution. 0.2 μm filtered 10× buffer stocks (5.5 μl) were mixed into test vials. Formulated samples were incubated at 22.6°C in an HPLC temperature-controlled injector compartment. The rhIL-15 deamidation rates were measured using ExRP-HPLC. To obtain degradation rate constants, single-component exponential decay curves were fit to the data trends using least-squares methods (Trendline Function, Microsoft Excel 2003).

## Variant Preparation

Methods for producing rhIL-15 and its variants were adapted from methods used for production of GMP-compliant rhIL-15 (5,6).

### *Mutagenesis*

Plasmid pET28-rhIL15 (5) containing the mature, human rhIL-15 coding sequence (Gene ID: 3600, Genebank: AAA21551.1) was subjected to site-directed mutagenesis (Quickchange, Agilent), following the manufacturer's instructions. The mutagenic oligonucleotide sequences used in this study were 52-bp long for single-point substitutions or 72-bp long for triple-point substitutions (Eurofins MWG Operon). Fourteen cycles were carried out with an extension time of 13 min, followed by treatment with DpnI, and transformation (1 μl) into *E. coli* DH10B-competent cells. Transformants were grown in Superior Broth (AthenaES, Baltimore, MD) supplemented with 50 μg/ml kanamycin. Plasmid DNA was prepared using a Qiaquick Mini Spin kit (Qiagen, Valenica, CA). DNA integrity was verified by agarose gel electrophoresis and restriction map analysis. Clones of the correct size were sequence-verified throughout the rhIL-15 sequence and the promoter regions.

### *Cell Culture*

LB medium having 10 g/L of Soytone (Catalog Number [C/N] 50209–481, Friesland Campina Domo, The Netherlands), 10 g/L of yeast extract (C/N 212750, Becton Dickinson, Franklin Lakes, NJ), and 10 g/L NaCl; and LB agar having LB+7.5 g/L agar (C/N 10147, Difco, KS) were autoclaved, cooled to 50°C, and 29 mg/L of 0.2 μm filtered kanamycin added. Cell banks of transformed BL21-AI™ chemically competent *E. coli* (C/N C6070, Invitrogen, CA) in 20% v/v glycerol (vegetable-based, C/N 2143, J.T. Baker, NJ) were stored below −70°C. For cell culture, autoclaved superbroth medium (12 ml/L glycerol, 12 g/L Soytone, 24 g/L yeast extract), was supplemented with 0.2-μm filtered stocks: 10× phosphates (38 g/L $KH_2PO_4$, 125 g/L $K_2HPO_4$); 100× $MgSO_4$ with antifoam (8 g/L $MgSO_4 \cdot 7\ H_2O$, 10 ml/L polypropylene glycol P2000, C/N 81380, Fluka; 0.2 μm filtered at 2–8°C), and 1000× antibiotic (29 mg/ml kanamycin). A 50-mL, 16-hour seed culture was split 1:100 into baffled fermentation flasks (5 L total volume). After 4 h at 37°C and 220 rpm, the $OD_{600}$ exceeded 3.0. Three hours after induction (1 mM IPTG, C/N Alx-582-001, Dioxane-free, Alexis Biochemical, NY; and 0.2% L-Arabinose, C/N A-3256, Sigma Aldrich, MO) cells were harvested by centrifugation and stored below −70°C.

### *Recovery and Refolding*

Standard methods (21,22) were adapted for recovery and refolding. Cell paste dispersed in TES buffer (50 mM Tris-HCl, 20 mM EDTA, 100 mM NaCl, pH 8.0) with 25% sucrose was homogenized six times at 700–900 bar (GEA Niro Soavi, Parma, Italy). The harvested inclusion bodies (IB) (Beckman JA-10, 9,000 rpm, 4°C, 30 min) were washed with TES+ 5% Triton X-100, rinsed with TES, and solubilized for 1 h (5 ml/g IB of 50 mM Tris-HCl, 5 mM EDTA, 8 M guanidine HCl, pH 8.5, and 100 mM freshly added DTT). Residual IB pellets (Beckman JA-20, 9,500 rpm, 4°C, 30 min) were re-solubilized. Combined supernatants were filtered (0.2 μm, Millipak-20,

MPGP02001 Millipore, MA) and loaded onto a Superdex 200 PG column (GE Healthcare, 5×88 cm, 4% CV load volume) pre-equilibrated with 6 M guanidine HCl, 5 mM EDTA, pH 6.3, and eluted at 30 cm/hour with UV monitoring at 280 nm. The pool was concentrated to 32 ml (Centriprep YM-10, Millipore, Billerica, MA) and refolded by drop-wise dilution with vigorous stirring over 20 min, into 1 L of chilled buffer (100 mM Tris, 2 mM EDTA, 500 mM L-Arginine, pH 9.5 with 0.6 g freshly added oxidized glutathione and 0.3 g freshly added reduced glutathione). After a further 20 min, the pH was adjusted to 7.4 with 50% HCl, and the conductivity was increased, targeting 1.2 M NaCl (122 mS/cm) with 100 mM Tris, 2 mM EDTA, 500 mM L-Arginine, 4 M NaCl, pH 7.4. The solution (1.4 L) was chilled overnight.

### *Purification*

HIC and IEX fraction purities were monitored using both SDS-PAGE and RP-HPLC. For each variant, new HIC resin (Toyopearl Butyl-650S, Tosoh Bioscience, 1.6×10 cm) was equilibrated with 3 column volumes (CV) of 100 mM Tris, 2 mM EDTA, 500 mM L-Arginine, and 1.2 M NaCl, pH 7.4. Refolded rhIL-15 was loaded at 240 cm/hour, followed by 3 CV of equilibration buffer, then 3 CV of 20 mM Tris, 1.2 M NaCl, pH 7.4. The flow rate was reduced to 60 cm/hour and the column developed with a 10-CV gradient of 20 mM Tris, 100 mM guanidine HCl, pH 7.4. The HIC pool was stored below −70°C. For each variant, new IEX resin (Source15Q, 15 µm, GE Healthcare, 1.6×8.5 cm bed) was equilibrated with 3 CV of argon-sparged 50 mM Tris, 1 mM EDTA, 100 mM NaCl, pH 7.4. The column was notably incubated at 32°C (EcoTherm C030, Torry Pines Scientific, Carlsbad, CA). The HIC pool was adjusted to 11±1 mS/cm with argon-sparged 50 mM Tris, 1 mM EDTA, pH 7.4, and loaded onto the IEX column at 150 cm/hour, followed by 10-CV equilibration buffer. A 30-CV elution gradient was run at 90 cm/hour up to 60% argon-sparged IEX buffer B (50 mM Tris, 1 mM EDTA, 1 M NaCl, pH 7.4). The IEX pool was held chilled.

### *Finishing*

The concentration of each IEX pool was measured by SEC-HPLC relative to a 0.56 mg/ml rhIL-15 reference standard that had been previously determined using the Coomassie Plus assay (C/N 23236, Pierce Biotechnology, IL; standardized *versus* 2 mg/ml BSA standard). IEX-stage pools were concentrated (YM-10 Centriprep, C/N 4305, Millipore) to 0.3 mg/ml. In a laminar flow biosafety cabinet, pools were 0.2-µm filtered (Millex-GV, Sterile, 0.22 µm, C/N SLGV013SL, Millipore), filled into autoclaved polypropylene vials with septum-closures, and stored below −70°C.

## RP-ESI-MS

To confirm variant preparation identities, a Waters Micromass QToF Premier quadrupole time-of-flight mass spectrometer (QToF) interfaced with a Waters Acquity ultra-high performance liquid chromatography system was used for intact mass measurement. A gradient of 0.9% B/min (A: 0.1% aqueous formic acid; B: 0.1% formic acid in acetonitrile) was used with an Acquity UPLC BEH C18 (1 mm×100 mm) column. The column was heated to 40°C. Mass spectrometer conditions: capillary was 2.5 kV; sampling cone was 45 volts; source temperature was 100°C; desolvation temperature was 200°C; and desolvation gas flow was 350 L/min. Samples were prepared in 50 mM ammonium carbonate, pH 7.0, and concentrated 15-fold (Centricon YM-3, Millipore).

## Variant Stress Testing

Aseptically filled rhIL-15 variant preparations in septum-closed, autoclaved plastic vials were simultaneously incubated at 37°C for 7 days within an Agilent HPLC temperature-controlled injector tray. At intervals the total percentage of non-deamidated rhIL-15 remaining in each preparation was measured using the fast cycle RP-HPLC method. Exponential decay curves were fit to the data trends using Microsoft Excel 2003, and degradation rates were obtained for each rhIL-15 variant.

## CTLL-2 Proliferation Assay

Cytotoxic T-Lymophocyte-2 cells, (ATCC, TIB-214, mouse) were used to assay rhIL-15 mediated cell stimulatory activity, as reported in a prior study (20). MTS, ([3-(4,5-dimethylthiazol-2-yl)-5-(3-carboxymethoxyphenyl)-2-(4-sulfophenyl)-2H-tetrazolium), and 125 µg/ml phenozine methosulfate (Promega, C/N PR-G3580) provided a colorimetric response (490 nm) proportional to the number of viable cells. Samples had residual endotoxin levels below 1 EU/mg by the kinetic Limulus Amoebocyte Lysate method (Lonza Rockland, ME). Absorbance data collected at 490 nm were fit using a log-logit 4-parameter curve using SoftMax Pro software (Molecular Devices).

# RESULTS AND DISCUSSION

## Overview

Control of deamidated rhIL-15 levels was sought through optimizing deamidation assays; improving process efficiency; investigating deamidation rates *versus* common process parameters; identifying the predominate deami-

dation site; and genetically substituting residues at that site. Successful deamidation control was confirmed by analytically comparing variant rhIL-15 with unmodified rhIL-15.

## Confirmation of rhIL-15 Deamidation

It was observed that recombinant human IL-15 (rhIL-15) became deamidated during customary production and use conditions. Deamidation detection within rhIL-15 was facilitated through the use of tandem-plumbed small-bead RP-HPLC columns eluted with shallow gradients, referred to as the ExRP-HPLC method (see Materials and Methods). ExRP-HPLC analysis of rhIL-15 preparations revealed two emergent major peaks (Fig. 1). This profile was similar to profiles for hexapeptides containing deamidated asparagine residues (13). The expected average molecular weight for rhIL-15 was 12900.6 AMU. RP/ESI-MS analysis confirmed the presence of rhIL-15 with a molecular weight of 12900.2 AMU, along with a major putatively deamidated species having a molecular weight of 12901.3 AMU. This was consistent with an amide ($-CONH_2$) deamidation to form a carboxyl group (–COOH) but was inconsistent with alternative protein degradations, including disulfide bond reduction (+2 AMU), oxidation (+16 AMU), or peptide hydrolysis (+18 AMU). The detection of isoaspartic acid in a protein is an indicator of possible deamidation (13). When deamidated rhIL-15 preparations were treated with protein isoaspartate methyltransferase (PIMT) (23) and assayed by RP-HPLC, a new methylated rhIL-15 peak was observed to increase in relative size at the expense of one of the major deamidated rhIL-15 species (Fig. 2, peak B). Further, the proportion of a second rhIL-15 deamidation peak (Fig. 2, peak D) increased relative to the amount of non-deamidated rhIL-15 (Fig. 2, peak N) with an observed shift in the N/D ratio from 2.64 to 2.12. This was consistent with slow conversion

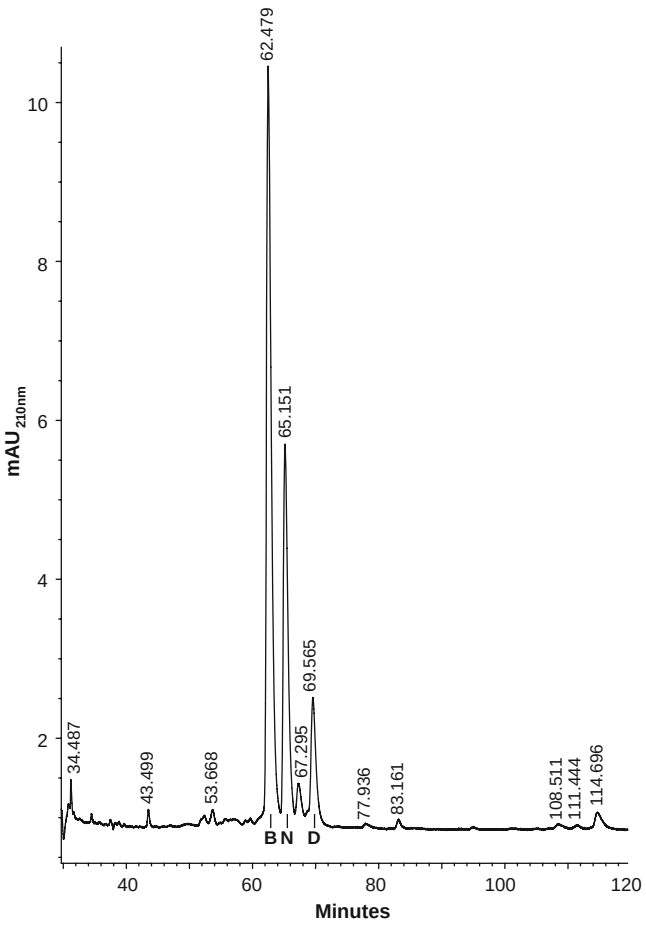


**Fig. 1** ExRP-HPLC analysis of partially deamidated rhIL-15. 'N', non-deamidated rhIL-15; 'B', isoaspartate form of deamidated rhIL-15; 'D', aspartate form of deamidated rhIL-15.

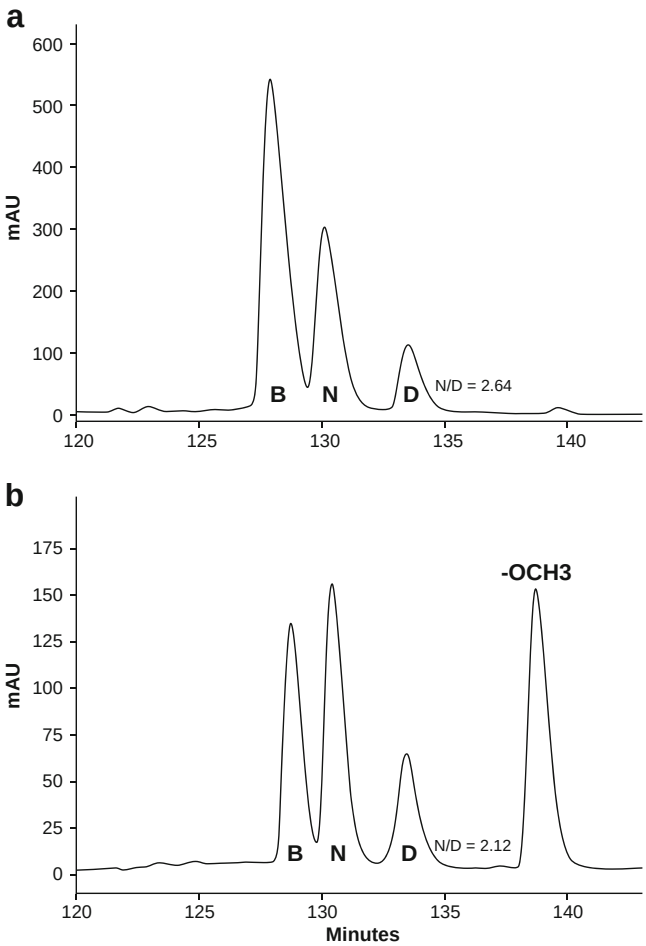


**Fig. 2** PIMT methylation of rhIL-15 isoaspartate-containing peaks. (**a**) RP-HPLC analysis of a partially deamidated rhIL-15 sample before reaction. (**b**) Analysis after enzymatic methylation using PIMT. Peak identifications: 'N', Non-deamidated rhIL-15; 'B', isoaspartate deamidated rhIL-15; 'D', aspartate deamidated rhIL-15; '-OCH3', methylated isoaspartate rhIL-15. The emergence of the methylated peak corresponded to a decrease in the size of peak 'B', confirming 'B' as the isoaspartic acid containing rhIL-15 substrate for reaction with PIMT.

of methylated isoaspartic rhIL-15 acid into an aspartic rhIL-15 form, following spontaneous demethylation (23). Control reactions containing rhIL-15 and the reaction mixture with either PIMT or S-adenosyl-L-methionine omitted showed no new peaks (data not shown, DNS). Taken together, RP-HPLC/ESI-MS and enzymatic methylation RP-HPLC suggested that deamidation contributed to the observed rhIL-15 heterogeneity.

## Motivation for Deamidation Control

Impacts of rhIL-15 deamidation on the CTLL-2 Proliferation Assay *in vitro* bioactivity assay were not observed within the range of assay variability (DNS). Deamidation may have effects *in vivo* that are not detected by an *in vitro* bioactivity assay, including pharmacokinetic and immunological impacts. Irrespective of whether such effects occur, the presence of significant deamidated rhIL-15 levels would complicate the clear assignment of clinical outcomes, positive and negative, to non-deamidated rhIL-15. This necessitated control of deamidated rhIL-15 levels as an important product purity/quality attribute for materials being produced for potential therapeutic use. Significantly, deamidated rhIL-15 complicated manufacturing operations, as resolution from non-deamidated rhIL-15 placed stringent demands on the performance and operation of chromatographic separation stages and potentially decreased process yields though the need for aggressive chromatographic peak fractionation (5,6).

## Transient Pair Suppression

For characterization and purification, efficient chromatographic methods were desirable. Deamidation shifted the calculated rhIL-15 isoelectric point from 4.52 to 4.45 (24). Separation of proteins differing by a single negative charge is practical (25). However, isolation of non-deamidated rhIL-15 using preparative IEX produced overlapping elution zones (DNS). To obtain sufficient sample purity, conservative peak fraction pooling that lowered process yields was required. To improve separations, rhIL-15 solution-state dynamics were analyzed. When rhIL-15 (0.3 mg/ml) was characterized using an analytical SEC column run at 5°C, an apparent mixture of monomer and dimer rhIL-15 forms was observed (Fig. 3a). The intra-peak valley traced out a distinctive concatenoid shape. Between 12°C and 22°C, the dimer peak area decreased and the valley merged with the monomer peak. From 27°C to 32°C, the monomer peak sharpened, and from 32°C to 42°C the proportions of residual irreversible dimer relative to the monomer peak stabilized. This progression qualitatively matched one previously computed for species involved in transient monomer–pairing equilibria (26). At 22°C, lower

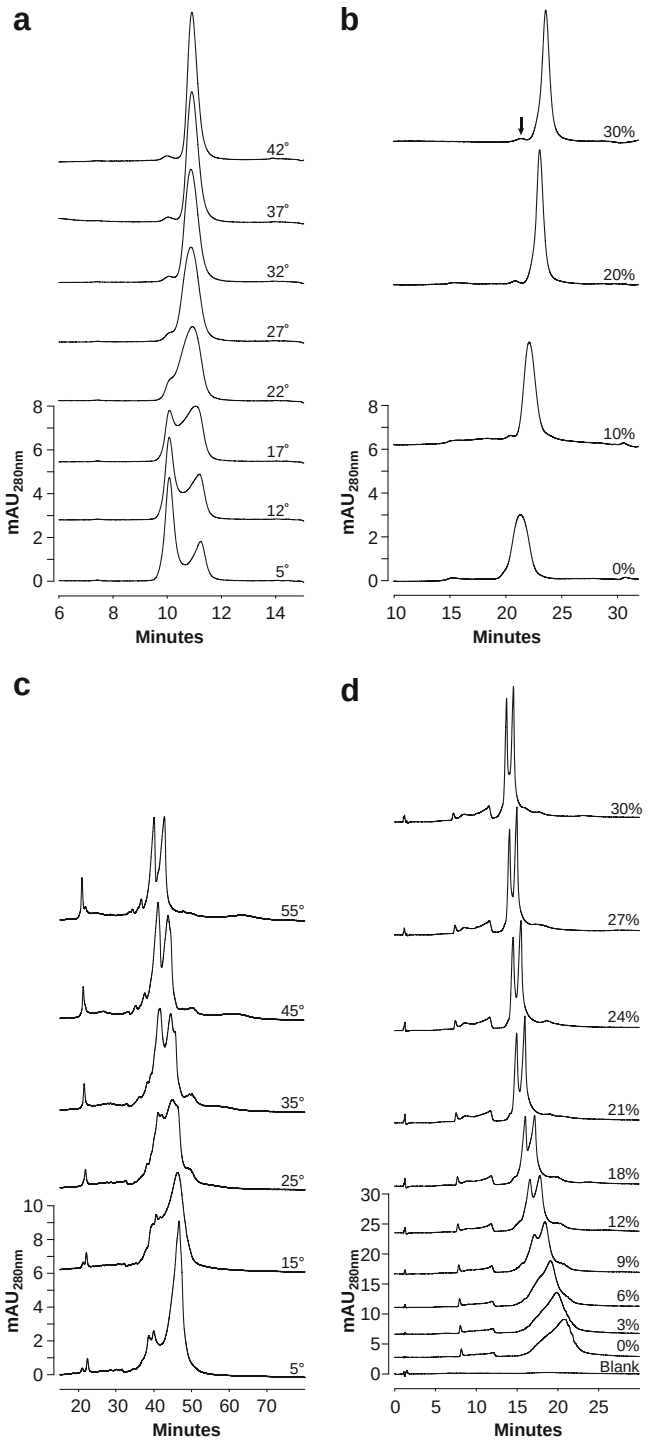


**Fig. 3** SEC and IEX chromatography profiles of partially deamidated rhIL-15 revealed complex elution behavior modulated by column temperature and mobile phase solvent composition. (**a**) SEC-HPLC—Analysis at 0.75 mL/min with aqueous buffer (no ethanol) under varying column temperature conditions. (**b**) Analysis at 0.375 mL/min and 22°C with varied mobile phase ethanol concentrations. (**c**) Analysis over Source 15Q resin with aqueous buffers and increasing column temperatures (5–55°C). (**d**) Analytical IEX-HPLC performed with ProPak SAX-10 column under constant temperature conditions with increasing ethanol concentrations (0–30% ethanol).

mass loading (obtained by sample pre-dilution or smaller injection volumes) increased the proportion of rhIL-15 monomer (DNS). This increase was consistent with mass-action modulation of a putative rhIL-15 monomer–pair competing equilibrium (26). At 22°C, adding ethanol to the mobile phase sharpened the monomer peak (Fig. 3b), with 20–30% ethanol being optimal. The rhIL-15 SEC peak shape was unchanged by varying the mobile-phase NaCl concentration from 0.150 to 0.5 M (DNS). Similarly, IEX analysis of partially deamidated rhIL-15, using aqueous-only buffers run at 5°C over preparative Source15Q resin, produced a broad major peak with two early-eluting minor peaks and a concatinoid valley (Fig. 3c). As temperatures increased, the profiles resolved into two sharp major peaks. Using an analytical IEX column (ProPak SAX-10), the impact of ethanol addition at 25°C was determined using the same rhIL-15 sample (Fig. 3d). With 0% ethanol, a broad, triangular peak was observed that resolved into two sharp peaks above 21% ethanol. Thus, it became clear that non-degraded and degraded rhIL-15 forms associated through hydrophobic interactions into a transient paired form (as distinct from traditional permanent dimer), that co-migrated during IEX separations.

## Transient Pairing Effects on Biological Assay and IEX Separation

As described above, rhIL-15 monomers transiently paired only under higher local concentrations and lower temperature conditions (Fig. 3a–d). Upon temperature increase or solvent addition, the equilibrium was shifted to favor the monomer. Given this equilibrium behavior, it was not feasible to evaluate the biological activity of the transiently paired rhIL-15 form as it would dissociate when isolated, when diluted into a bioassay, or when raised to physiological temperatures. Interest in dispersing paired rhIL-15 in a process context was focused on improving chromatographic removal of deamidated rhIL-15. Individual rhIL-15 molecules apparently interchanged between the two states while traveling down the length of the chromatography bed leading to substantial peak broadening and asymmetry. Further, transiently paired deamidated rhIL-15 and non-deamidated rhIL-15, would co-migrate for a time and prevent efficient separation. However, under conditions where rhIL-15 pairing was unfavorable, either through the addition of alcohols or the moderate elevation of process temperatures, IEX operated traditionally and optimal separation efficiency was observed. This restoration of chromatographic efficiency may potentially increase yields and improve removal of other host cell related contaminates that would otherwise co-purify within the range of the broadened rhIL-15 peak.

## Deamidation Kinetics Measurements

Deamidation in peptide hormones followed pseudo first-order kinetics (13–16). Kinetics studied with small molecules (27) may elucidate clear degradation pathways. However, due to the complexity of biomolecules and limitations of characterization methods, kinetic studies of intact whole proteins are infrequently reported. The high-resolution ExRP-HPLC assay (USP resolution factor ≥2.0) enabled dependable measurement of rhIL-15 deamidation, despite rhIL-15 being 10-fold larger than previously reported peptides. This method's extended cycle time and use of two tandem analytical columns provided the optimal resolution within the pressure range of our instrumentation. The kinetics studied in this report demonstrated a pseudo first-order chemical reaction for rhIL-15 deamidation with negligible residuals ($R^2 > 0.99$). This ExRP-HPLC method was used to determine the Arrhenius activation energy for rhIL-15 deamidation (Fig. 4). Using this method, 29

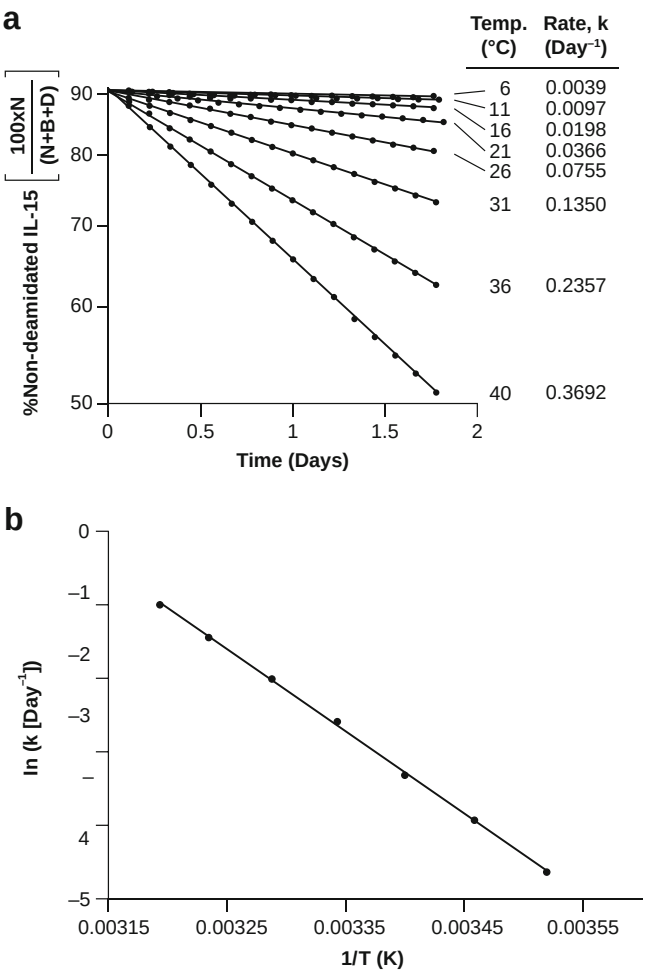


**Fig. 4** Effect of incubation temperatures on rhIL-15 deamidation rates. (**a**) Kinetic trends obtained in 25 mM sodium phosphate, 500 mM NaCl, pH 7.4, as measured using ExRP-HPLC. (**b**) Arrhenius plot determination of the rhIL-15 deamidation activation energy (22.9 kcal·mol$^{-1}$).

**a**

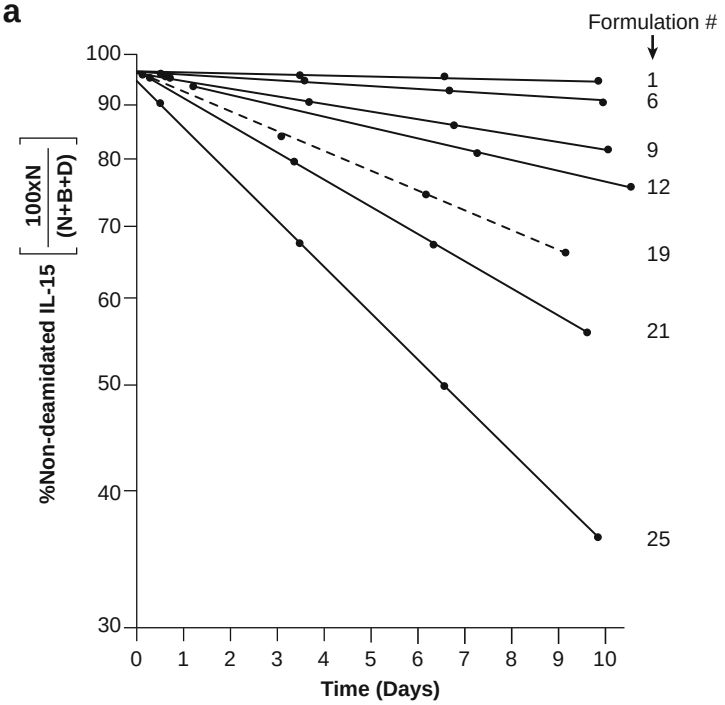


**b**

| Formulation | Buffer pH | Percent Recovery | $R^2$ | Deamidation Rate at 22.6°C ($Day^{-1}$) | Relative Deamidation Rate |
|---|---|---|---|---|---|
| **1. 25 mM Na Citrate, 500 mM NaCl** | **5.94** | **104** | **0.84** | **0.0013** | **0.03** |
| 2. 25 mM Na Acetate, 500 mM NaCl | 5.88 | 114 | 0.95 | 0.0030 | 0.08 |
| 3. 25 mM Bis-Tris Propane, 500 mM NaCl | 5.91 | 100 | 0.98 | 0.0033 | 0.08 |
| 4. 25 mM Na Cit., 1% Man., 1% Suc., 0.01% Tween 80 | 6.20 | 91 | 1.00 | 0.0040 | 0.10 |
| 5. 25 mM Imidazole, 500 mM NaCl | 5.90 | 130 | 0.99 | 0.0055 | 0.14 |
| **6. 25 mM Na Citrate, 500 mM NaCl** | **6.41** | **107** | **0.99** | **0.0058** | **0.15** |
| 7. 25 mM Bis-Tris Propane, 500 mM NaCl | 6.45 | 103 | 0.99 | 0.0093 | 0.24 |
| 8. 25 mM Imidazole, 500 mM NaCl | 6.40 | 101 | 0.99 | 0.0131 | 0.33 |
| **9. 25 mM Na Citrate, 500 mM NaCl** | **6.92** | **109** | **1.00** | **0.0155** | **0.39** |
| 10. 25 mM Bis-Tris Propane, 500 mM NaCl | 6.86 | 107 | 1.00 | 0.0187 | 0.47 |
| 11. 25 mM Tris, 500 mM NaCl | 6.90 | 111 | 1.00 | 0.0191 | 0.48 |
| **12. 25 mM Na Citrate, 500 mM NaCl** | **7.40** | **99** | **1.00** | **0.0215** | **0.54** |
| 13. 25 mM Na Phosphate, 1% Mannitol, 1% Sucrose | 7.40 | 103 | 1.00 | 0.0261 | 0.66 |
| 14. 25 mM Na Phosphate, 5% Glycerol | 7.40 | 116 | 1.00 | 0.0278 | 0.70 |
| 15. 25 mM Imidazole, 500 mM NaCl | 6.90 | 121 | 1.00 | 0.0318 | 0.80 |
| 16. 25 mM Bis-Tris Propane, 500 mM NaCl | 7.40 | 104 | 1.00 | 0.0331 | 0.84 |
| 17. 25 mM Tris, 500 mM NaCl | 7.40 | 106 | 1.00 | 0.0348 | 0.88 |
| 18. 25 mM Na Phosphate, 500 mM NaCl, 2% Mannitol | 7.40 | 121 | 1.00 | 0.0368 | 0.93 |
| *STARTING FORMULATION:* | | | | | |
| **19. 25 mM Na Phosphate, 500 mM NaCl** | **7.40** | **103** | **1.00** | **0.0396** | 1.00 |
| 20. 25 mM Na Phos., 500 mM NaCl, 1% Cyclodextran | 7.40 | 129 | 1.00 | 0.0419 | 1.06 |
| **21. 25 mM Tris, 500 mM NaCl** | **7.90** | **108** | **1.00** | **0.0539** | **1.36** |
| 22. 25 mM Na Phosphate, 50 mM Arginine | 7.40 | 108 | 1.00 | 0.0549 | 1.38 |
| 23. 25 mM Imidazole, 500 mM NaCl | 7.40 | 114 | 1.00 | 0.0579 | 1.46 |
| 24. 25 mM Na Phosphate, 250 mM NH4Acetate | 7.40 | 103 | 1.00 | 0.0639 | 1.61 |
| **25. 25 mM Tris, 500 mM NaCl** | **8.40** | **115** | **1.00** | **0.0941** | **2.37** |
| 26. 25 mM Citrate, 500 mM NaCl | 5.53 | 44.8 | Mass Lost – Invalid Trend | | |
| 27. 25 mM Acetate, 500 mM NaCl | 5.42 | 61.4 | Mass Lost – Invalid Trend | | |
| 28. 25 mM Na Phos., 250 mM Ammonium Sulfate | 7.40 | | Secondary Reaction – Invalid Trend | | |
| 29. 250 mM Na Phos., 500 mM NaCl, 2% Sucrose | 7.40 | | Secondary Reaction – Invalid Trend | | |

**Fig. 5** Effect of alternative buffer formulations on rhIL-15 deamidation rates. Kinetic trends obtained during incubation at 22.6°C measured using ExRP-HPLC. (**a**) Plot of the ExRP-HPLC deamidation ratio *versus* incubation time for selected formulations (shown in bold). (**b**) Trial formulations for rhIL-15 covering a pH range from 5.4 to 8.4.


**Fig. 6** rhIL-15 amino acid sequence with the first residue of the mature human sequence assigned as asparagine 1. Disulfide bonds link cysteine 35 to cysteine 85 and cysteine 42 to cysteine 88.

formulation conditions were simultaneously assayed (Fig. 5), demonstrating the practical utility of the method for measuring deamidation kinetics.

### *Deamidation Temperature Dependence and Process Design*

At process scales, sharpening IEX profiles through addition of ethanol to mobile phases would have required explosion-proof facility design and increased waste handling costs. Thus, use of elevated column temperatures to increase IEX efficiency was preferable. Measurement of rhIL-15 deamidation rates *versus* temperature was therefore of interest. Consistent with a prior report (28), the rate of rhIL-15 deamidation increased at elevated temperatures and followed classical Arrhenius kinetics with a calculated activation energy of 22.9 kcal·mol$^{-1}$ (Fig. 4). This result closely agreed with previously published deamidation activation energies of 27.8 and 22.0 kcal·mol$^{-1}$ for deamidation of oxytocin (15) and insulin (16), respectively. Thus, when running IEX columns at 32°C, the on-column rate of rhIL-15 deamidation would increase 35-fold relative to 6°C. Although the total elevated temperature exposure time could be minimized through process design, elevated temperatures would be problematic if unexpected on-column processing delays occurred. Therefore, elevated process temperatures could be used only if the base-line rate of rhIL-15 deamidation was decreased.

### *rhIL-15 Deamidation Rates Decreased under Mildly Acidic Conditions*

rhIL-15 deamidation kinetics were measured at 22.6°C for a range of buffer compositions (Fig. 5). Consistent with previous studies (11), solution pH significantly influenced rhIL-15 deamidation. At pH ≤5.5, rhIL-15 precipitated (Fig. 5, Formulations [F-] 26 and 27). At and above pH 5.9, rhIL-15 remained soluble. In citrate buffer, deamidation was 17-fold slower at pH 5.9 than at pH 7.4 (Fig. 6, F-1, F-12). Similarly, lower pH conditions slowed deamidation for rhIL-15 formulated in Bis-Tris-Propane (F-3, F-7), Imidazole (F-5, F-15), and Tris (F-17, F-21, F-25) buffers. At pH 7.4, the deamidation rate was slowest in citrate buffer and fastest in Imidazole buffer (citrate<Bis-Tris-Propane<Tris<Phosphate<imidazole; F-12, F-16, F-17, F-19, F-23). rhIL-15 deamidation rates increased by a factor of 2.4-fold as solution pH increased from pH 7.4 to pH 8.4 (F-19, F-25). Arginine and ammonium acetate moderately accelerated deamidation (F-22, F-24, F-19), while mannitol, sucrose,

**Table I** Peptide Mapping of the Primary rhIL-15 Deamidation Site. MS/MS Collision-dissociation of the Chymotryptic Fragment Having m/z = 1101.80 ES+, or an $MH^+$(monoisotopic) mass of 3303.4, Corresponding to Peptide A70-F99. The Calculated b-ion and y-ion Values were Derived Assuming Residue 77 to be an Aspartic Acid, Representing a Deamidated Asparagine Residue

| Fragment ID | | Calculated b-ion | Observed b-ion | Ion Charge | Fragment ID | | Calculated y-ion | Observed y-ion | Ion Charge |
|---|---|---|---|---|---|---|---|---|---|
| b | | | | | y | | | | |
| 1 | A | – | N/M | | 30 | A | – | N/M | |
| 2 | N | 186.0873 | 186.08 | (+1) | 29 | N | 3232.4256 | N/M | (+2) |
| 3 | N | 300.1302 | 300.11 | (+1) | 28 | N | 3118.3827 | 3118.18 | (+2) |
| 4 | S | 387.1623 | 387.14 | (+1) | 27 | S | 3004.3398 | 3004.14 | (+2) |
| 5 | L | 500.2463 | 500.22 | (+1) | 26 | L | 2917.3078 | 2917.14 | (+2) |
| 6 | S | 587.2784 | 587.24 | (+1) | 25 | S | 2804.2237 | 2803.80 | (+2) |
| 7 | S | 674.3104 | (691.21) | (+1) | 24 | S | 2717.1917 | 2717.02 | (+2) |
| 8 | D | 789.3373 | 789.28 | (+1) | 23 | D | 2630.1596 | 2629.98 | (+2) |
| 9 | G | 846.3588 | 846.30 | (+1) | 22 | G | 2515.1327 | 2514.96 | (+2) |
| 10 | N | 960.4017 | 960.33 | (+1) | 21 | N | 2458.1112 | 2457.96 | (+2) |
| 11 | V | 1059.4701 | N/M | | 20 | V | 2344.0683 | 2343.90 | (+2) |
| 12 | T | 1160.5178 | N/M | | 19 | T | 2244.9999 | 2244.88 | (+2) |
| 13 | E | 1289.5604 | N/M | | 18 | E | 2143.9522 | 2143.90 | (+2) |
| 14 | S | 1376.5924 | N/M | | 17 | S | 2014.9096 | 2014.78 | (+2) |
| 15 | G | 1433.6139 | N/M | | 16 | G | 1927.8776 | 1927.72 | (+2) |
| 16 | C | 1536.6231 | N/M | | 15 | C | 1870.8561 | 1869.72 | (+2) |

and glycerol moderately slowed deamidation (F-13, F-14, F-18, F-19). However, using 1% sucrose by itself led to the emergence of unique rhIL-15-related species, detected as sharp, early-eluting peaks in ExRP-HPLC profiles (F-29, DNS). These presumed sucrose adducts were not observed when either 1% mannitol with 1% sucrose, or 1% mannitol alone were used. A lyophilization-compatible formulation significantly slowed rhIL-15 deamidation (F-4). Thus, the use of mildly acidic conditions in combination with a citrate buffer slowed rhIL-15 deamidation. These mildly acidic formulations may be useful for extended rhIL-15 administration if low-pH stocks were mixed in-line just prior to infusion with a physiological, buffered saline solution. However, the use of mildly acidic conditions was not ideal for stabilizing rhIL-15 in-process. As lowered pH conditions approach the rhIL-15 isoelectric point ($pI$=4.5), the binding strength of rhIL-15 toward IEX resin weakens and rhIL-15 solubility decreases. Thus, a genetic engineering approach to controlling rhIL-15 deamidation was investigated.

## Identification of N77 as a Significant Deamidation Site

The rhIL-15 amino acid sequence is shown in Fig. 6, with the first asparagine in the mature, native rhIL-15 sequence assigned as the first amino acid (29). At pH ≥4.0, steric bulk contributed by the amino acid following an asparagine residue impacts deamidation rates by hindering the formation of a key succinimide deamidation intermediate (9). The relative asparagine deamidation rates in model hexapeptide systems have been previously explored (9). Although asparagine deamidation rates are modified by protein secondary and tertiary structures (30), it was reported that pentapeptide deamidation rates are similar to deamidation rates for similar motifs within unhindered regions of proteins (10). Examination of Protein Data Bank structure 2Z3Q (31) revealed that the nine rhIL-15 asparagines occur on surface-exposed, relatively unencumbered alpha-helices or loop regions, suggesting that pentapeptide deamidation rates might be applicable to rhIL-15. As tabulated by Robinson and coworkers (10), if the nine asparagine residues in rhIL-15 had been present in glycine-terminated pentapeptides, the following relative deamidation half-lives would be predicted: (M-N1-W) 93 d; (V-N4-V) 291 d; (E-N65-L) 130 d; (S-N77-G) 0.96 d; (G-N79-V) 224 d; (K-N95-I) 313 d; and (I-N112-T) 46 d. Deamidation rates for double asparagine motifs were estimated through replacing asparagine with aspartic acid in the underlined position: (A-N71-N) 32 d and (N-N72-S) 17 d. Notably, the predicted deamidation rate for the (S-N77-G) motif was the fastest of all possible motifs. Because there were two orders of magnitude difference between the fastest and slowest Robinson motifs found within rhIL-15, modifying a subset of the least stable motifs was hypothesized to slow overall rhIL-15 degradation. To determine if there was in fact such a limited set of highly unstable deamidation sites, chymotryptic digestion, followed by RP-HPLC peptide mapping and ESI-MS analysis, was used to detect peptides covering all nine asparagine residues (DNS, in elution order: I111-S114; E53-N65; M0-W2; E53-L66; S76-F99; A70-F99; S73-F99; Q48-L66; I67-F99; I68-L100; E53-L69). Isotopic fine structures that were shifted 1 AMU relative to the expected peptide weight highlighted peptides A70-F99, I67-F99, and I68-L100 as possibly containing deamidated asparagines. MS/MS fragmentation of the deamidated A70-F99 peptide revealed b- and y-ion series that were consistent with deamidation at asparagine 77 (Table I). This analysis provided empirical confirmation that asparagine 77 was a likely unstable rhIL-15 deamidation site.

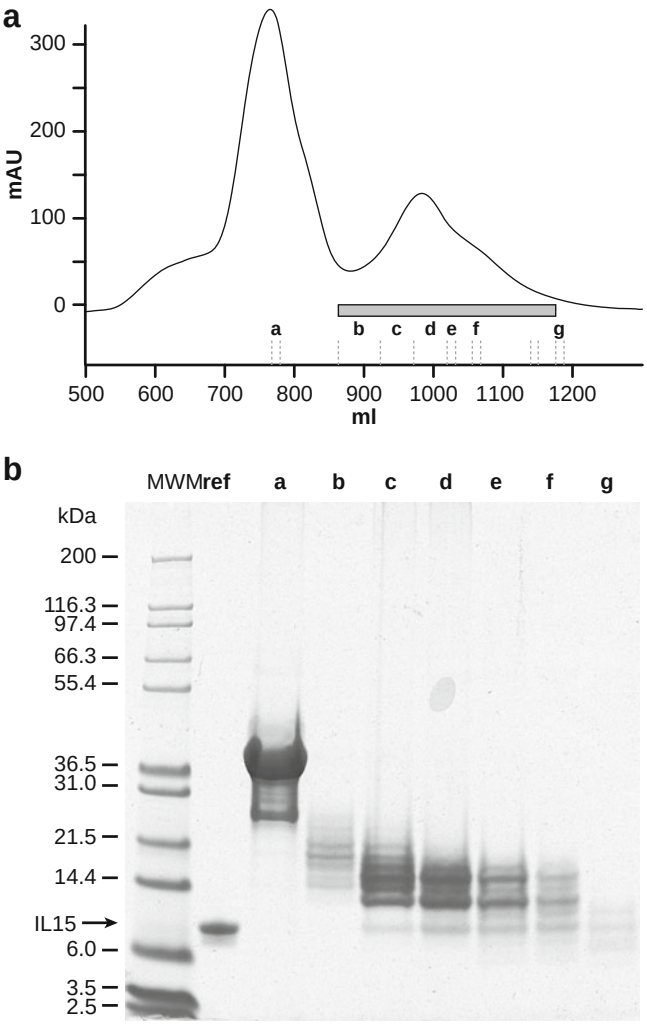


**Fig. 7** Purification of reduced, denatured rhIL-15 N77A using SEC. (**a**) SEC elution profile. Peak fractions b–g (shaded box) were pooled for further processing. (**b**) Reduced, Coomassie blue-stained, SDS-PAGE analysis: MWM, Molecular weight markers; ref, reduced rhIL-15 reference standard; a–g, respective ethanol precipitated SEC column fractions.

### Genetic Substitutions of rhIL-15

The three predicted most unstable motifs containing N77, N71, and N72 are located in surface-exposed regions of rhIL-15 that are distal from the rhIL-15 alpha-receptor binding interface (31). While this suggested that the overall structure and function of rhIL-15 might be maintained after conservative substitutions at one or more of these positions, the actual impacts of such substitutions on deamidation resistance and on potency within a cellular context had to be determined empirically. Therefore, five rhIL-15 mutants were created to provide the greatest possibility of successfully identifying a functional rhIL-15 variant. The alanine (N77A) and serine (N77S) variants represented low-steric hindrance hydrophobic and hydrophilic amino acid substitutions. The glutamine (N77Q) variant extended the side chain by one methylene group while maintaining a polar-amide end group. The glutamine residue was predicted to exhibit pentapeptide deamidation rates of >500-fold slower than asparagine (10). The G78A variant hindered formation of a succinamide intermediate considered necessary for asparagine deamidation (12) and was predicted to slow deamidation in pentapeptides by 25-fold (10). To determine if multiple substitutions were needed to obtain sufficient solution stability, the triply substituted (N71S/N72A/N77A) variant was constructed.

### Preparation of rhIL-15 Variants

Preparation of rhIL-15 variants followed methods adapted from methods for manufacture of GMP-compliant rhIL-15 at the 500 milligram per batch scale (5,6); a scale sufficient to meet initial clinical trial material demand for this highly potent interleukin. Process modification to replace urea with guanidine for HIC elution prevented the possibility of lysine carbamylation interfering with comparison of rhIL-15 forms. Practical and scalable elevation of the IEX process temperature improved IEX stage separation efficiency. Thus, the process methodology changes that are described below would be practical at the 500 mg production scale and may perhaps simplify future engineering scale-up as material demand increases.

For brevity, the N77A preparation is shown as representative of all the variant preparations. rhIL-15 was produced in *E. coli*, recovered as inclusion bodies, and solubilized using guanidine HCl. Inclusion-body extracts were purified using SEC under denaturing conditions (Fig. 7a). Target rhIL-15 was observed as a minor band, with an anomalous apparent molecular weight of 8 kDa, which eluted below a complex set of intense host–cell protein bands (Fig. 7b, Fractions c–f). Anti-rhIL-15 Western blot analysis (DNS) detected only trace rhIL-15 dimer and multimer migrating between the host–cell protein

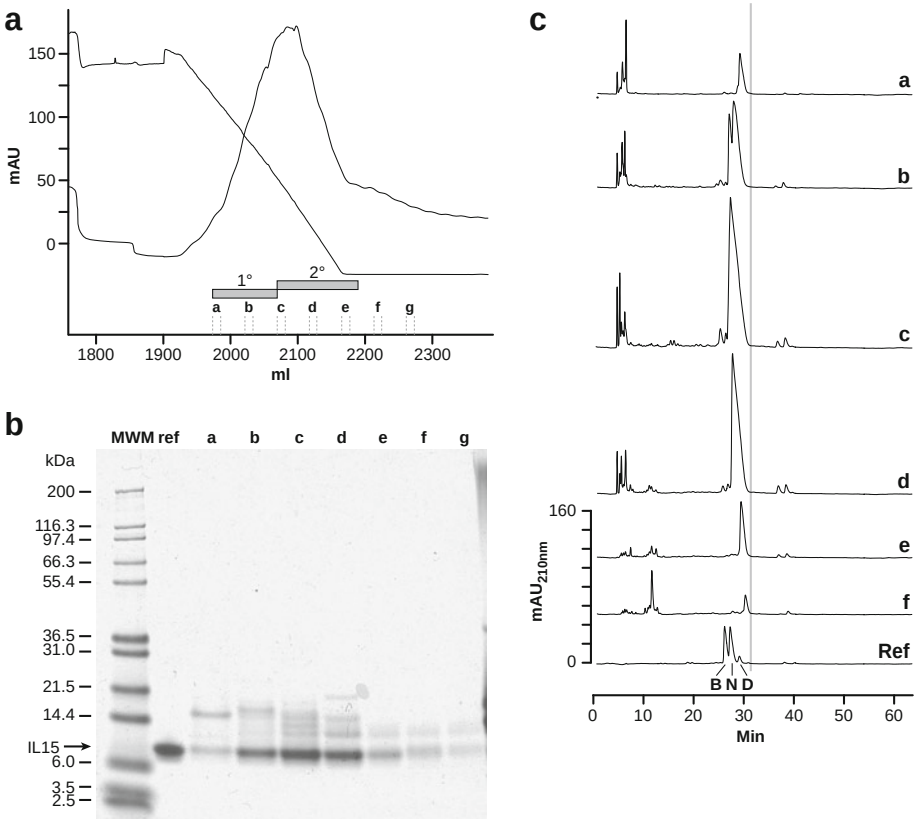


**Fig. 8** HIC purification of refolded rhIL-15 N77A over Toyopearl Butyl-650S resin. (**a**) HIC elution profile. Fractions were pooled and processed as two pools (1° and 2°, shaded boxes). (**b**) Reduced, Coomassie blue-stained, SDS-PAGE analysis: MWM, Molecular weight markers; ref, reduced rhIL-15 reference standard; a–g, respective HIC column fractions. (**c**) HIC elution fractions 'a' through 'f' were analyzed by Rapid RP-HPLC (60 min cycle, Poroshell column method). The gray line marks the invariant rhIL-15 N77A peak tail retention time. Ref, Partially deamidated, unsubstituted rhIL-15 that eluted characteristically earlier than rhIL-15 N77A.

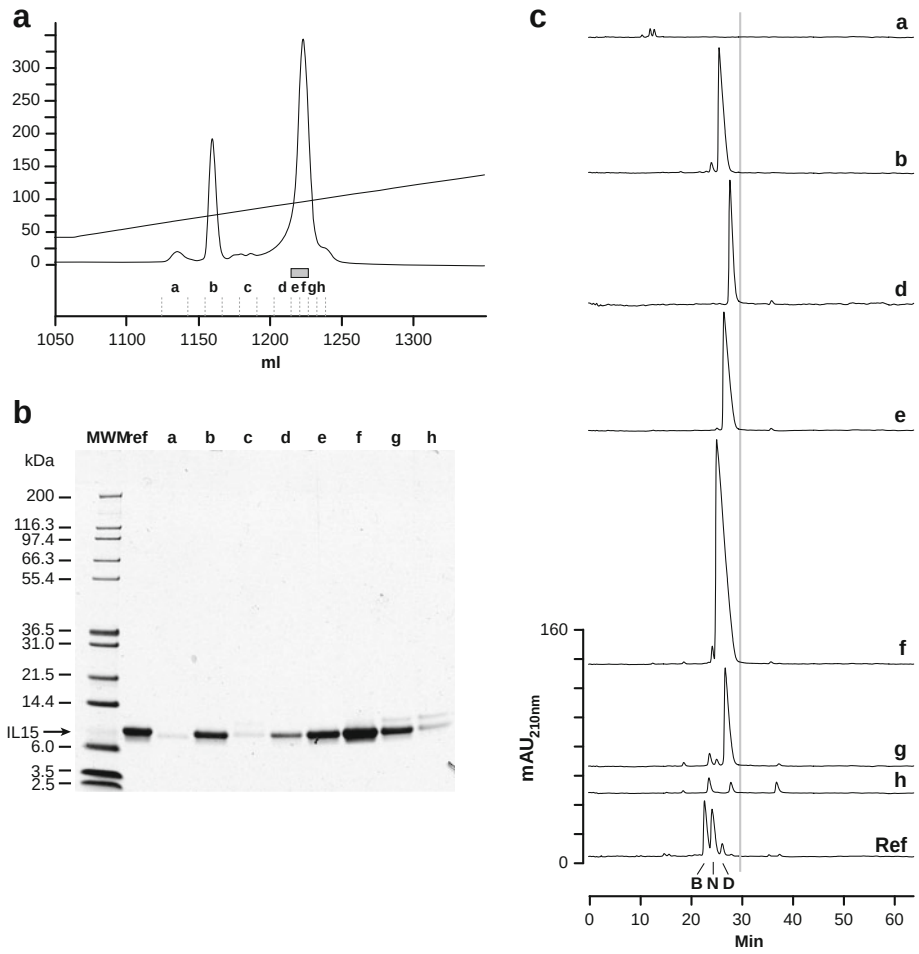


**Fig. 9** IEX purification of refolded rhIL-15 variant N77A over Source15Q resin held at 32°C. (**a**) IEX elution profile from processing of secondary HIC pool. Peak center fractions e and f were pooled. An rhIL-15-related contaminant peak, b, was excluded. (**b**) Coomassie blue-stained SDS-PAGE analysis: MWM, Molecular weight markers; ref, reduced rhIL-15 reference standard; a-h respective IEX column fractions. (**c**) RP-HPLC analysis of selected HIC elution fractions a–g. Early- and late-eluting contaminant species observed in HIC fractions (Fig. 8) were absent from IEX stage fractions. The gray line marks the invariant rhIL-15 N77A peak tail retention time. Ref, Partially deamidated, unsubstituted rhIL-15 that eluted characteristically earlier than rhIL-15 N77A.

bands (Fig. 7b, fractions c–f) and so confirmed the majority of rhIL-15 to be monomeric. SEC-purified rhIL-15 was reliably refolded by a 45-fold drop-wise dilution in the presence of a 1:1 w/w oxidized- to reduced-glutathione redox couple. Refolded rhIL-15 was purified using HIC (Fig. 8a). SDS-PAGE and RP-HPLC analysis revealed substantial rhIL-15 enrichment (Fig. 8b,c). IEX chromatography run at 32°C (Fig. 9a) recovered rhIL-15 as a sharp major peak (Fig. 9a, fractions e and f) that was well separated from contaminants (Fractions a, b, c, h). Minor deamidated rhIL-15 species eluted after the main rhIL-15 peak (Fig. 9c, fraction h), consistent with an extra negative charge binding them more tightly to the positively charged resin. The predominant, unidentified contaminant (Fig. 9a, fraction b) was indistinguishable from the target rhIL-15 species using SDS-PAGE (Fig. 9b) and MS analysis (DNS). However, using RP-HPLC, the contaminant differentially eluted between the early deamidated rhIL-15 peak and the major non-deamidated rhIL-15 peak (Fig. 9c, fraction b). The concentrated IEX main peak fractions were pooled (Fig. 9a, fractions e and f) and concentrated. The purified preparation identities were confirmed using ESI-MS analysis (Table II). The purities of the preparations were comparable using SEC-HPLC (Table III), SDS-PAGE (Fig. 10), and RP-HPLC (Fig. 11a, top panes). Modification of SEC-HPLC analysis using orthogonal approaches, ethanol addition or column temperature elevation, dispersed transient rhIL-15 pairs, and so enabled measurement of the permanent dimer forms that will most likely exist within a physiological context where the rhIL-15 will be both highly diluted and at 37°C. No relationship was observed between the extent of transient monomer/pair equilibrium and permanent dimer formation or aggregation. RP-HPLC retention times increased for the N77A and

**Table II** Confirmation of Final rhIL-15 Preparation Identities Using ESI-MS Analysis

| Identity | MS-ESI | Expected | Difference |
|---|---|---|---|
| Unsubstituted | 12898.34 | 12900.7 | −2.36 |
| N77A | 12855.91 | 12857.68 | −1.77 |
| N77S | 12872 | 12873.68 | −1.68 |
| N77Q | 12913 | 12914.73 | −1.73 |
| G78A | 12912.8 | 12914.73 | −1.93 |
| 3M | 12786.17 | 12787.6 | −1.43 |

**Table III** Comparison of Final rhIL-15 Preparation Monomer Percentages. Comparisons Were Performed Under Two Conditions Known to Disperse rhIL-15 Transient Pairs

| Identity | Percent Monomer 22°C, 20% Ethanol | Percent Monomer 37°C, No Ethanol |
|---|---|---|
| Unsubstituted | 99.6 | 99.2 |
| N77A | 99.9 | 99.7 |
| N77S | 99.6 | 99.0 |
| N77Q | 94.8 | 94.1 |
| G78A | 99.1 | 98.4 |
| 3M | 99.6 | 98.8 |

(N71S/N72A/N77A) variants, consistent with substitution of hydrophobic alanine for polar asparagine residue(s). These tests confirmed the six preparations had comparable and acceptable purities for accelerated stress testing.

## Genetic Substitutions Eliminated Primary Deamidation

The six rhIL-15 variant preparations formulated in 50 mM Tris, 1 mM EDTA, 300 mM NaCl, at pH 7.4 were subjected to accelerated stress testing at 37°C for seven days, followed by repetition of RP-HPLC analysis (Fig. 11a, lower panes). Unsubstituted rhIL-15 deamidated rapidly, producing a characteristic triplet. However, a predominant single peak remained for each variant after elevated-temperature stress testing. This demonstrated the marked relative stability of the rhIL-15 variants. The variants did accumulate minor species during stress testing, being <5% of the total peak area. The N77A, N77S, and N77Q variants were similarly stable, except that N77A and N77S variants displayed a trace singlet peak emergent just before the main rhIL-15 peak, whereas N77Q produced a doublet. The G78A variant showed a complex accumulation of minor species on both sides of the main peak, consistent with continued but slower deamidation at N77. Two minor peaks emerged at retention times of 20 and 22 min in the unsubstituted, N77A, N77S, N77Q, and G78A rhIL-15 test samples. For the (N71S/N72A/N77A) or "3M" variant, the corresponding peak region, would have been shifted (see above) to 26 min. However, peaks in this region were attenuated, suggesting that the peaks that were seen in the single-substitution variants may have arisen from deamidation at N71 or N72. Thus, based upon RP-HPLC results, the (N71S/N72A/N77A)-rhIL-15 variant was the most stable variant, followed by the N77A-rhIL-15 variant.

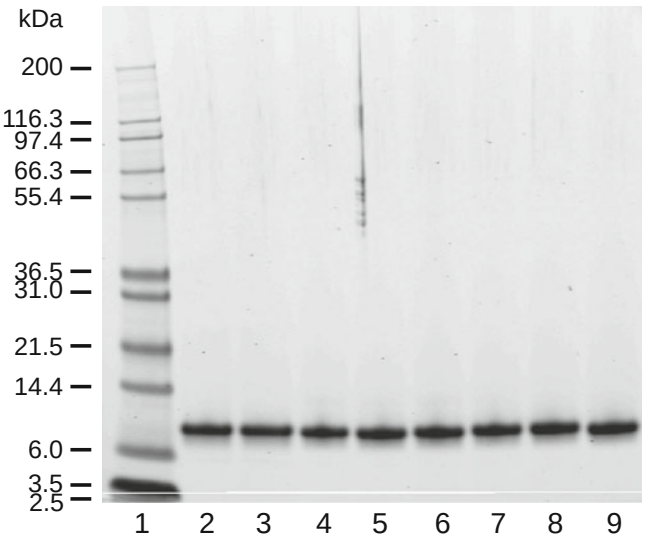


**Fig. 10** Sypro Ruby SDS-PAGE analysis of the rhIL-15 variant preparations demonstrating comparable purities. Loading was 1 $\mu$g/lane. Lane 1, Mark 12 molecular weight markers; lanes 2 and 3, Unsubstituted rhIL-15 reference standard; lane 4, Unsubstituted rhIL-15 prepared similarly to variant forms; lane 5, rhIL-15 N77A; lane 6, rhIL-15 N77S; lane 7, rhIL-15 N77Q; lane 8, rhIL-15 G78A; lane 9, rhIL-15 (N71S/N72A/N77A) or "3M".

## Kinetic Comparisons of rhIL-15 Stabilities

To quantitatively measure variant stabilities, the preparations were simultaneously subjected to accelerated stress testing (Fig. 11b). The variant degradation measurements were based on the percentage of non-degraded rhIL-15 relative to all peaks detected within the effective RP-HPLC assay range. This approach monitored all forms of degradation, including secondary degradations that may have been revealed by deletion of the primary deamidation site. A shorter RP-HPLC cycle, performed using pellicular-bead resin, was used to generate deamidation profiles for wild type and five variants (Fig. 11b). Specifically, the peak areas for the six rhIL-15 variant preparations were measured on 18-hour intervals and the main peak percentages were plotted *versus* incubation time. Exponential decay curves were fit to the data and the total degradation rate constants were calculated. The rhIL-15 variants were essentially stable over the course of accelerated stress testing, with <5% of rhIL-15 degraded over the seven-day span of the test. However, greater than 75% of the originally present unsubstituted rhIL-15 degraded under identical conditions. With trends fit to single-phase exponential decay curves using automated least squares methods, the kinetic decay constants for the rhIL-15 variants were found to be comparable with rates of k=0.0056, 0.0043, 0.0071, 0.0029, and 0.0071 day$^{-1}$ for N77A, N77S, N77Q, G78A, and (N71S/N72A/N77A) variants, respectively. However, unsubstituted rhIL-15 degraded with a rate constant of 0.17 day$^{-1}$. Thus, the rhIL-15 variants were >23-fold more stable than unsubstituted rhIL-15.

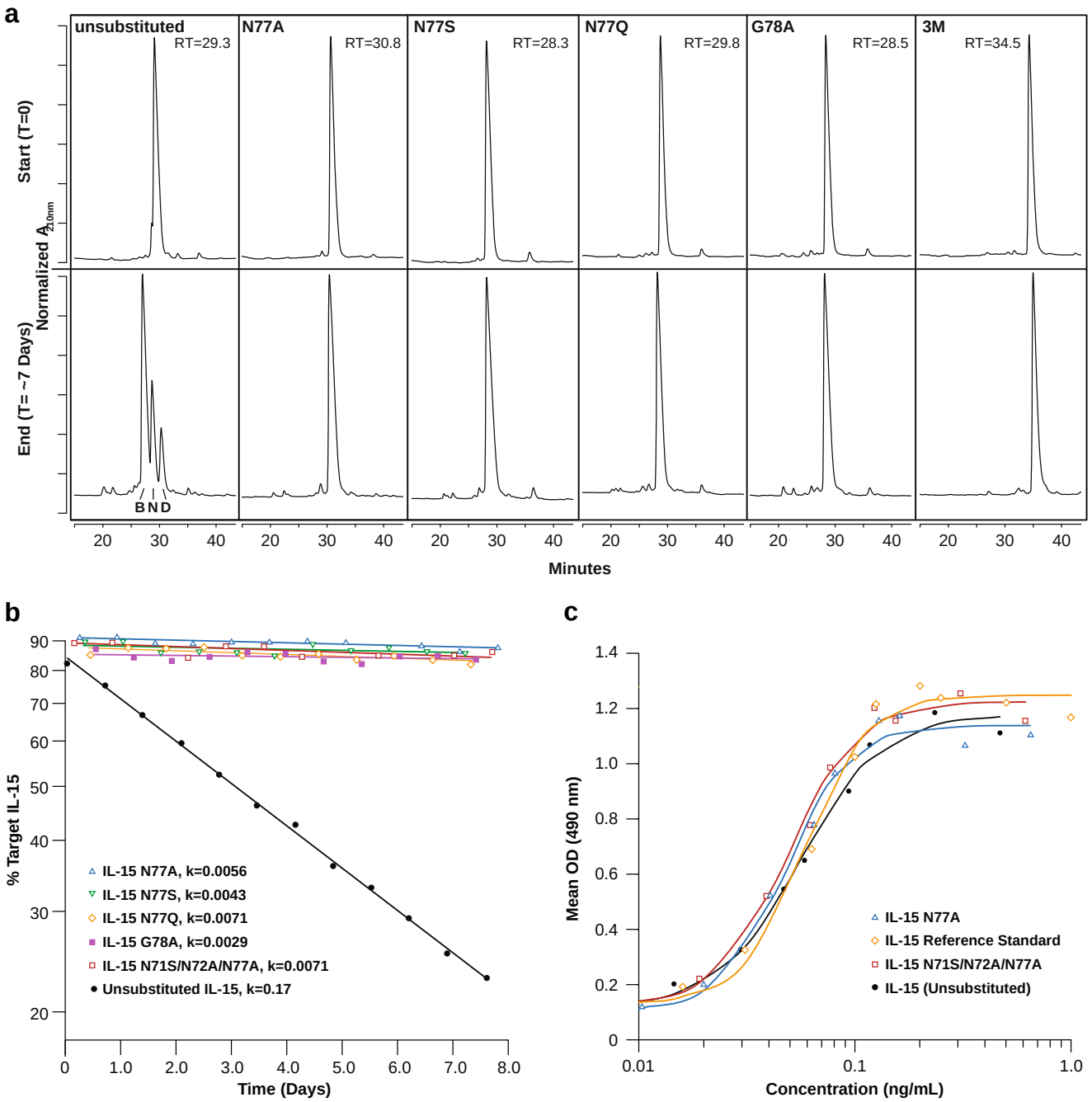


**Fig. 11** Analysis of rhIL-15 variant preparations. (**a**) Accelerated stress testing, RP-HPLC assay at the start and end of incubation at 37°C for 7 days, in 50 mM Tris, 1 mM EDTA, 250 mM NaCl, pH 7.4. Main peak intensities were normalized to full scale. Characteristic variant retention times are shown. (**b**) Quantitative kinetic stability assessment (37°C for 7 days) using RP-HPLC analysis. Trends for unsubstituted rhIL-15 and the five rhIL-15 variant preparations are identified (inset), along with respective deamidation rate constants. (**c**) Cell proliferation potency (CTLL-2) evaluation of selected rhIL-15 variants. Proliferation rends for rhIL-15 reference standard, unsubstituted rhIL-15, rhIL-15 N77A variant and rhIL15 (N71S/N72A/N77A) variant are identified (inset).

## rhIL-15 Variants Retained Potency

The N77A and (N71S/N72A/N77A) rhIL-15 variants, the unsubstituted rhIL-15, and a previously produced rhIL-15 reference standard, were assayed *in vitro* for a cytotoxic T-cell (CTLL-2) proliferation (20) (Fig. 11c). In each case, a concentration of 0.05 ng/mL of rhIL-15 was sufficient to increase cell growth by 50% relative to the maximum cell growth observed at 0.2 ng/mL of rhIL-15. Thus, when assayed side by side, reference standard rhIL-15 preparations, unsubstituted rhIL-15 produced in this study, the N77A rhIL-15 variant, and the (N71S/N72A/N77A) rhIL-15 variant displayed equivalent potencies.

## CONCLUSIONS

Heterogeneity in rhIL-15 preparations was originally observed using RP-HPLC methods and assigned as deamidation based on intact molecule RP-ESI/MS analysis and a PIMT/RP-HPLC peak-shift assay. Characterization and purification of rhIL-15 benefited from improved chromatographic efficiencies obtained either by adding 20% ethanol as a co-solvent or by raising the column temperature to ≥32°C. To further understand rhIL-15 stability, deamidation kinetics were measured under a range of temperatures, buffer compositions, and buffer pH conditions. At pH 7.4, the rhIL-15 deamidation reaction had an Arrhenius activation energy of 22.9 kcal·per mol. Lower pH formulation buffers slowed deamidation, with an optimally slow rate obtained in citrate buffer at pH 5.9. To fortify rhIL-15 against deamidation, peptide mapping was used to empirically identify the deamidation sites, with the primary deamidation site identified at asparagine 77. Amino acid substitutions were made to generate five mutants that were purified and further characterized in deamidation rate and biological activity assays. Substituting asparagine 77 was sufficient to eliminate the primary rhIL-15 deamidation reaction. Additional substitutions of asparagines 71 and 72 led to a modest increase in rhIL-15 stability. Alternatively, replacing glycine 78 with alanine impeded the primary deamidation reaction, leaving asparagine 77 intact, but was not as effective as the asparagine replacements. When held at 37°C, all of the rhIL-15 variants exhibited degradation rates that were >23-fold slower relative to the rate observed for unsubstituted rhIL-15. Critically, rhIL-15 variants (N77A and [N71S/N72A/N77A]) and unsubstituted rhIL-15 forms were equivalently active in a CTLL-2 proliferation activity assay, demonstrating maintenance of essential T-cell growth promotion after substitution. Thus, substitution of rhIL-15 at N77A and (N71S/N72A/N77A) led to functional preparations having substantially improved deamidation resistance. These variants minimized the potential for immunogenicity posed by deamidated product-related contaminants. The added thermal stability also facilitated purification under conditions that dispersed a putative transient rhIL-15 pair. This new material composition formed the basis of a practical and effective method to manufacture high-quality rhIL-15 variant preparations. These improved preparations will have particular value for clinical applications, where drug purity and stability are critical.

## ACKNOWLEDGMENTS & DISCLOSURES

This project has been funded in whole or in part with federal funds from the National Cancer Institute, National Institutes of Health, under contract HHSN261200800001E. The content of this publication does not necessarily reflect the views or policies of the Department of Health and Human Services, nor does mention of trade names, commercial products, or organizations imply endorsement by the U.S. government. This research was supported in part by the Developmental Therapeutics Program in the Division of Cancer Treatment and Diagnosis of the National Cancer Institute. We thank Samir Shaban for providing initial rhIL-15 preparations; Dr. Soman Gopalan and Dr. Timothy Veenstra for valued discussions; Tammy Schroyer and Allen Kane for scientific graphics support; Ashley DeVine for document editing; and Dr. Stephen Creekmore for valued guidance and manuscript review.

## REFERENCES

1. Shanmugham LN, Petrarca C, Frydas S, Donelan J, Castellani ML, Boucher W, *et al.* rhIL-15, an immunoregulatory and anti-cancer cytokine, recent advances. J Exp Clin Cancer Res. 2006;25(4):529–36.
2. Ridrigues L, Bonorino C. Role of rhIL-15 and rhIL-21 in viral immunity: applications for vaccine and therapies. Expert Rev Vaccines. 2009;8(2):167–77.
3. Cheever MA. Twelve immunotherapy drugs that could cure cancers. Immunol Rev. 2008;222:357–68.
4. Ward A, Anderson M, Craggs RI, Maltby J, Grahames C, Davies RA, *et al.* E. coli expression and purification of human and cynomolgus IL-15. Protein Expr Purif. 2009;68(1):42–8.
5. Vyas VV, Esposito D, Sumpter TL, Broadt TL, Hartley J, Knapp GC IV, Cheng W, Jiang M-S, Roach JM, Yang X, Giardina SL, Mitra G, Yovandich JL, Creekmore SP, Waldmann TA, Zhu J. Clinical manufacturing of recombinant human Interleukin 15: I. Production cell line development and protein expression in *E. coli* with stop codon optimization. Biotech Prog. 2011 (Submitted, Under Review).
6. Vyas VV, Jiang M-S, Burnette A, Nellis DF, Shaban S, Cheng W, Wu J, Sumpter TL, Broadt TL, Knapp GC IV, Roach JM, Giardina SL, Mitra G, Yovandich JL, Creekmore SP, Waldmann TA, Zhu J. Clinical manufacturing of recombinant human Interleukin 15: II. Clinical manufacturing process development. (To Be Submitted).
7. Fewkes NM, Mackall CL. Novel gamma-chain cytokines as candidate immune modulators in immune therapies for cancer. Cancer J. 2010;16(4):392–8.
8. Jakobisiak M, Golab J, Lasek W. Interleukin 15 as a promising candidate for tumor immunotherapy. Cytokine Growth Factor Rev. 2011. doi:10.1016/j.cytogfr.2011.04.001.
9. Patel K, Borchardt RT. Chemical pathways of peptide degradataion. III Effect of primary sequence on the pathways of deamidation of asparaginyl residues in hexapeptides. Pharm Res. 1990;7(8):787–93.
10. Robinson NE, Robinson ZW, Robinson BR, Robinson AL, Robinson JA, Robinson ML, *et al.* Structure-dependent nonenzymatic deamidation of glutaminyl and asparaginyl pentapeptides. J Peptide Res. 2004;63:426–36.
11. Wakankar AA, Borchardt RT. Formulation considerations for proteins susceptible to asparagine deamidation and aspartate isomerization. J Pharm Sci. 2006;95(11):2321–36.
12. Catak S, Monard G, Aviyente V, Ruiz-López MF. Deamidation of asparagine residues: direct hydrolysis *versus* succinimide-mediated deamidation mechanisms. J Phys Chem A. 2009;113(6):1111–20.
13. Geiger T, Clark S. Deamidation, isomerization, and racemization at asparaginyl and aspartyl residues in peptides, succinimide-

linked reactions that contribute to protein degradation. J Biol Chem. 1987;262(2):785–94.
14. Sasaoki K, Hiroshima T, Kusumoto S, Nisi K. Deamidation at asparatine-88 in recombinant human interleukin-2. Chem Pharm Bull (Tokyo). 1992;40(4):976–80.
15. Hawe A, Robert P, Stefan R, Kasper P, Van der Heijden R, Jiskoot W. Towards heat-stable oxytocin formulations: analysis of degradation kinetics and identification of degradation products. Pharm Res. 2009;26(7):1679–88.
16. Dotsikas Y, Loukas YL. Kinetic degradation study of insulin complexed with methyl-beta cyclodextrin. Confirmation of complexation with electrospray mass spectrometry and 1H NMR. J Pharm Biomed Anal. 2002;29:487–94.
17. Eggleton P, Haigh R, Winward PG. Consequences of neo-antigenicity of the 'altered self'. Rheumatology. 2008;47:567–71.
18. Doyle HA, Gee RJ, Mamula MJ. Altered immunogenicity of isoaspartate-containing proteins. Autoimmunity. 2007;40(2):131–7.
19. Pepinsky RB. Selective precipitation of proteins from guanidine hydrochloride-containing solutions with ethanol. Anal Biochem. 1991;195:177–81.
20. Soman G, Yang X, Jiang H, Giardina S, Vyas V, Mitra G, *et al.* MTS dye-based colorimetric CTLL-2 cell proliferation assay for product release and stability monitoring of interleukin-15: assay qualification, standardization and statistical analysis. J Immunol Methods. 2009;348(1–2):83–94.
21. Palmer I, Wingfield PT. Preparation and extraction of insoluble (inclusion-body) proteins from *Escherichia coli*. Curr Protoc Protein Sci. 2004;6.3.1−6.3.18.
22. Wingfield PT, Palmer I, Liang S-M. Folding and purification of insoluble (inclusion-body) proteins from *Escherichia coli*. 2001 Curr Protoc Protein Sci. 6.5.1−6.5.27.
23. Johnson BA, Aswad DW. Optimal conditions for the use of protein l-isoaspartyl methyltransferase in assessing the isoaspartate content of peptides and proteins. Anal Biochem. 1991;192:384–91.
24. Gasteiger E, Hoogland C, Gattiker A, Duvaud S, Wilkins MR, Appel RD, *et al.* Protein identification and analysis tools on the ExPASy server. In: Walker JM, editor. The proteomics protocols handbook. New York: Humana Press; 2005. p. 571–607.
25. Nellis DF, Ekstrom DL, Kirpotin DB, Zhu JW, Andersson R, Broadt TL, *et al.* Preclinical manufacture of an anti-HER2 scFv-PEG-DSPE, liposome-inserting conjugate. 1. Gram-scale production and purification. Biotechnol Prog. 2005;21:205–20.
26. Stevens FJ. Analysis of protein–protein interaction by simulation of small-zone size exclusion chromatography; Stocastic formulation of kinetic rate contributions to observed high-performance liquid chromatography elution characteristics. Biophys J. 1989;55:1155–67.
27. Zhu J, Zhang S, Tong C. Studies on the kinetics of deacetylcephalosporin C (DCPC) decomposition rate. Pharmaceutical Industry (Chinese). 1985;16:481–6.
28. Stratton LP, Kelly R, Rowe J, Shively JE, Smith DD, Carpenter JF, *et al.* Controlling deamidation rates in a model peptide: effects of temperature, peptide concentration, and additives. J Pharm Sci. 2001;90(12):2141–8.
29. Grabstein KH, Eisenman J, Sheanebeck K, Rauch C, Srinivasan S, Fung V, *et al.* Cloning of a T-cell growth factor that interacts with the beta chain of the interleukin-2 receptor. Science. 1994;264 (5161):965–8.
30. Robinson NE. Protein deamidation. Proc Natl Acad Sci U S A. 2002;99(8):5283–8288.
31. Chirifu M, Hayashi C, Nakamura T, Toma S, Shuto T, Kai H, *et al.* Crystal structure of the rhIL-15-rhIL-15Ralpha complex, a cytokine-receptor unit presented in trans. Nat Immunol. 2007;8(9):1001–7.